COR1 Engineering Test Unit Measurements at the Mauna Loa Solar Observatory, September 2003

William Thompson
Nelson Reginald
Kim Streander

October 9, 2003

1 Introduction

The COR1 Engineering Test Unit (ETU), which had been previously tested at the NCAR/HAO and NRL test facilities, was modified into an instrument capable of observing the Sun. It was then taken to the Mauna Loa Solar Observatory to observe the corona.

The changes made to observe the Sun were as follows:

- The plate scale was changed to accommodate the smaller Apogee camera. This change had already been made for the NRL tests.
- The previous Oriel polarizer was replaced with a commercial Polarcor polarizer from Newport to be more flight-like. However, because of cost and availability considerations, this polarizer was smaller than those which will be used for flight.
- A structure was placed around the back section of the instrument, to protect it from stray light.
- A pointing spar borrowed from HAO was used to track the Sun.

A few days into the test, it became evident that some artifacts were appearing in the data, and these artifacts were changing as the polarizer was rotated. It was decided to test two other polarizers, the Oriel polarizer which had been used in the previous tests at HAO and NRL, and a Nikon polarizer which was borrowed from a camera belonging to one of the observatory staff members. These three polarizers had much different qualities, as shown below.

2 Calibration

The calibration window that will be in the instrument door on the flight instrument was simulated by mounting a diffuser and neutral density filter in front of the objective. These were identical materials to those which will be used in the door, although they were not glued together into a single optic. Instead, they were pressed together into the flight configuration. The resulting flat field image is shown in Figure 1.

From these data, we can derive a calibration to apply to the scattered light measurements. The diffuser window was measured to have a BTDF of 0.1305 sr^{-1}. Given the solar diameter of

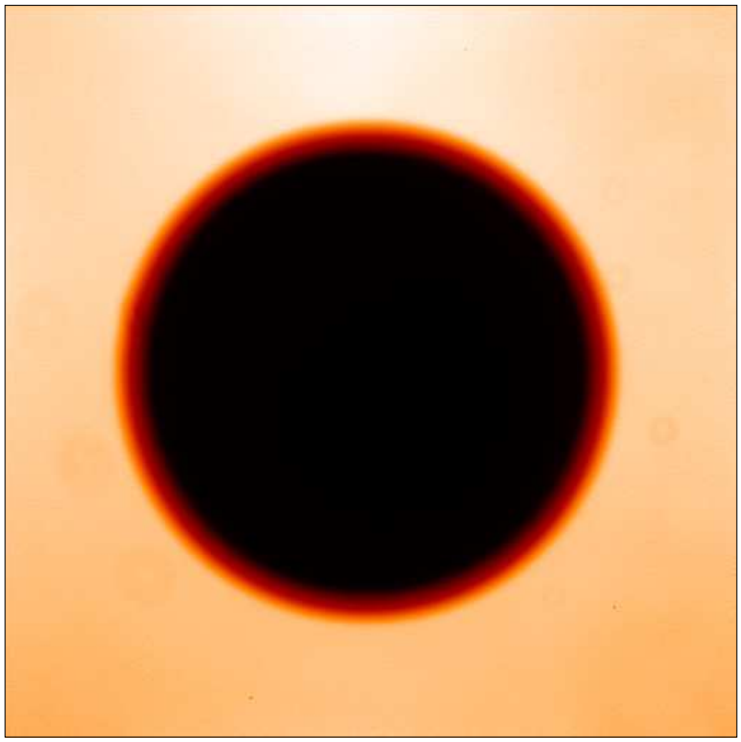

Figure 1: Flat field image.

953 arc seconds during the observation, and taking the 1.0 ND neutral density filter into account, this means that the instrument was exposed to light of $8.75 \times 10^{-7} B/B_{\odot}$. At an exposure time of 0.02 s, which was used for the bulk of the observations, the average signal was 9938.86 counts. Thus, the conversion from counts to $B/B_{\odot}$ can be established.

Some variation is seen in the calibration as a function of exposure time. Observations were made at 0.02 s, 0.05 s, and 0.1 s. The calibration derived at 0.02 s and 0.05 s are 18% and 4% higher respectively than that derived from the 0.1 s exposure. It's believed that these variations are caused by the non-flight shutter, which was operating at the extreme edge of its capability. There's also an excess brightness feature at the top of the flat field image which seems to be independent of exposure time, and probably represents a non-uniformity caused by the shutter.

One important question is whether the instrument is properly designed to fit within the exposure capabilities of the flight detector and shutter. The Apogee camera has a digitization of 5 electrons per count. When this is applied to the 0.1 s exposure results, and the slight difference in plate scale is taken into account, we calculate that a camera with a full well capacity of 4×10^5 electrons exposed to a signal of $10^{-6} B/B_{\odot}$ would saturate after about 0.2 s. However, the flight bandpass filters will be much narrower than the filter in the ETU. Taking this into account increases the maximum possible exposure time to 0.6–0.7 s. The COR1 instrument specification calls for this number to be between 0.1–1.0 s. Therefore, this condition is well met.

Figure 2 shows an image of the Sun partially off the occulter. It was taken by putting a couple of neutral density filters (4.0D and 2.0D) in front of the objective. From this image, we can establish that the plate scale is 8.69 arcsec/pixel, or 0.36 arcsec/μm. This is slightly larger than the flight design of 7.5 arcsec/pixel, or 0.28 arcsec/μm. The plate scale was increased to accommodate the

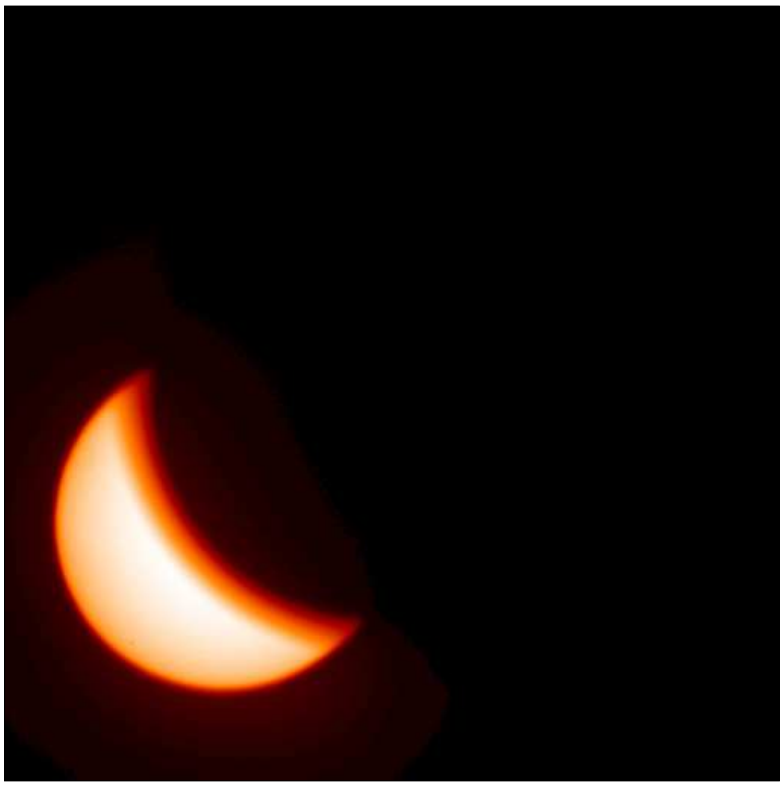

Figure 2: Image of the Sun partially off the occulter.

smaller non-flight Apogee camera.

It should be noted that the apparent solar brightness in Figure 2 is about a factor of 10 brighter than would be implied by the 10^{-6} extinction expected of the combined filters. This effect was also seen in the NRL tests, and the filters are not considered to be reliable for calibration purposes. If the filters were used for calibration, the scattered light levels derived below would be a factor of 10 *lower*. In other words, the scattered light would be lower than one could possibly expect.

3 Scattered light

Figure 3 shows a typical image of the scattered light levels seen in the instrument. The average radial trace through these data is shown in Figure 4. We see that the two bright rings around the edge of the occulter are consistent with the brightnesses seen in the previous lab measurements. However, the overall level of scattered light is much higher than what was seen in the lab. This is due to the additional atmospheric scatter, and is consistent with the expectations at this site.

Considerable variation was seen in the scatter level as a function of time. Figure 5 shows the number of counts as a function of time on two separate areas of the detector, one on the bottom and the other on the left side. These data were taken with the polarizer removed from the optical train, so are unaffected by any polarization characteristics of the instrument. It's evident that the scattered light level is subject to sudden changes. Not only does the overall level of scattering change, but the shape of the scatter profile can also change, as shown by the fact that the two

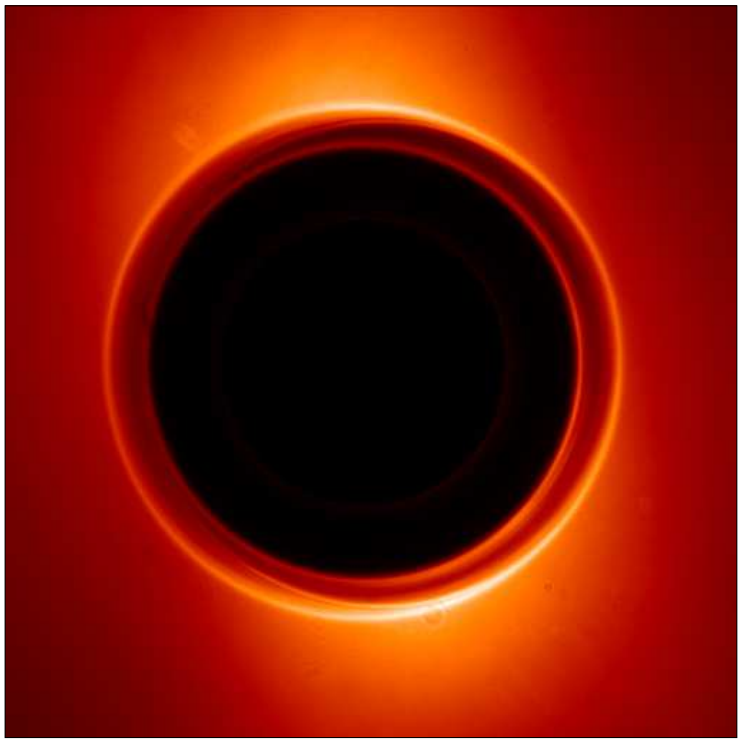

Figure 3: Typical scattered light image.

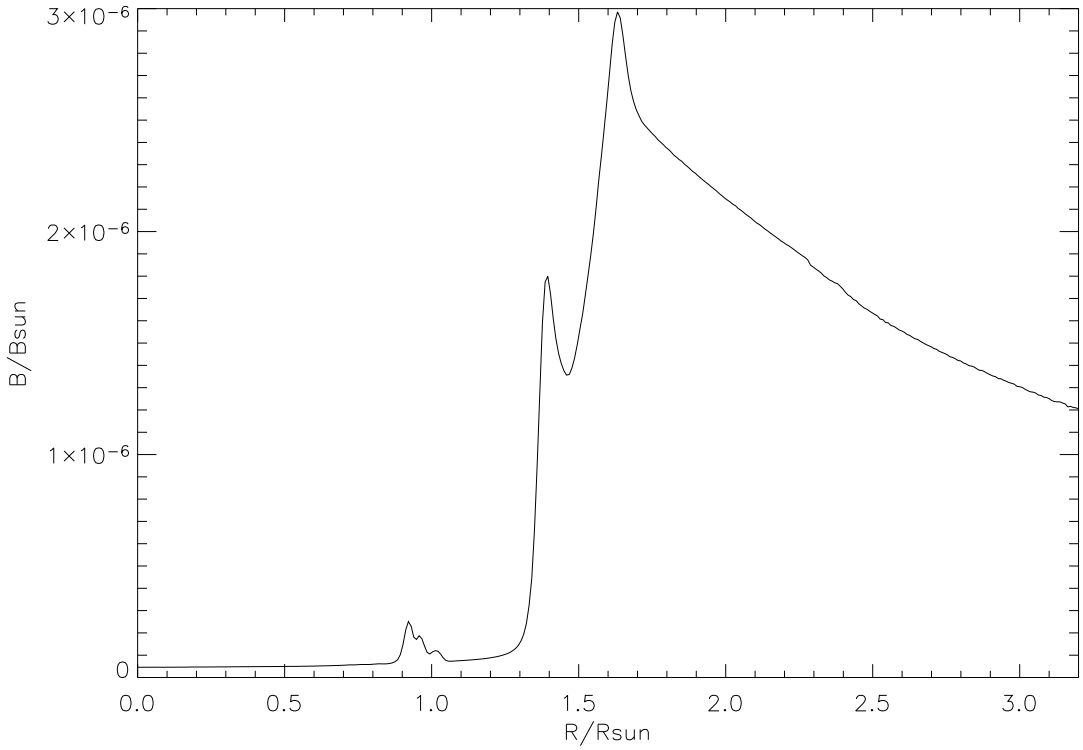

Figure 4: Typical plot of scattered light as a function of radial distance.

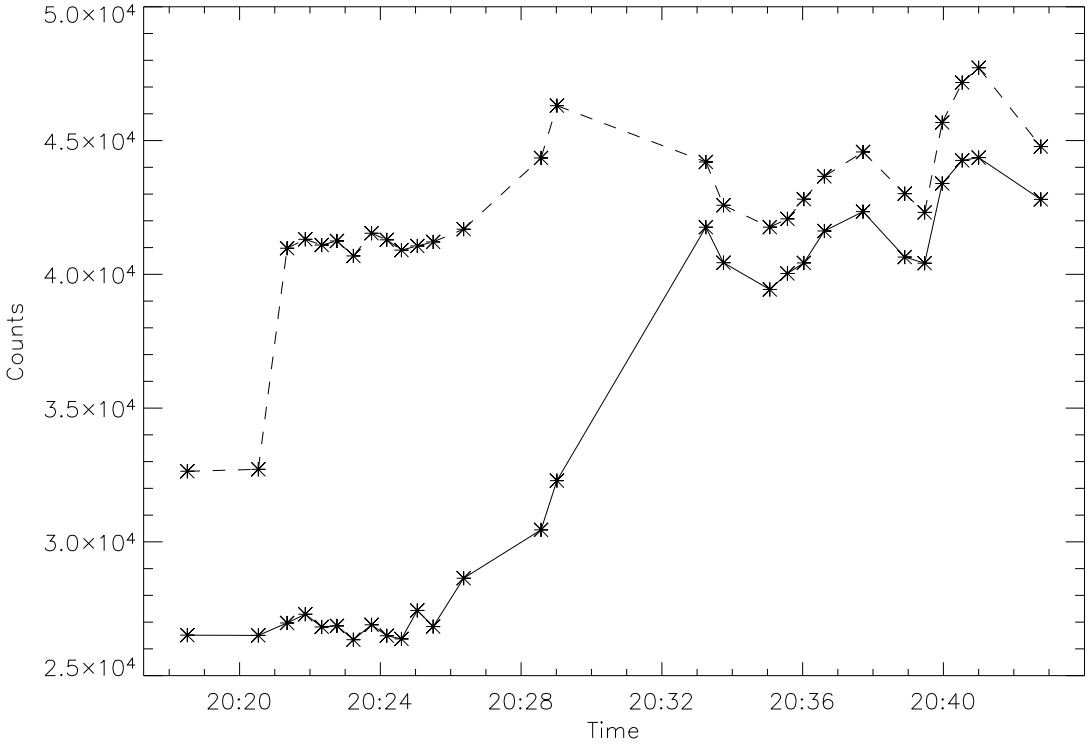

Figure 5: Scattered light level as a function of time for two areas on the detector. The dashed line represents an area toward the bottom of the detector, while the solid line represents an area on the left side.

curves do not follow each other. The sudden changes most likely represent large single pieces of dust which settled on the objective. At times, the scattered light would start to saturate the detector, and it would become necessary to pause operations to blow the dust off of the objective.

It was found necessary to attach a baffle to the front of the instrument to shield it from light scattered from structures around the instrument.

4 Image motions

4.1 Jitter

It's evident from looking at movies of the data that the instrument is subjected to a fair amount of jitter. The magnitude of this jitter can be measured by coaligning the scatter pattern between images. Previous observations at HAO showed that the scatter pattern follows the solar image. To coalign the images, it's first necessary to mask off the bright rings around the edge of the occulter, which are not subject to instrument jitter. A cross-correlation matrix is then built up between image pairs, and a bi-lateral Gaussian function of the form

$$G = A_0 + A_1 \exp\left(-(\frac{x-x_0}{A_4})^2 - (\frac{y-y_0}{A_5})^2 - A_6(x-x_0)(y-y_0)\right) \quad (1)$$

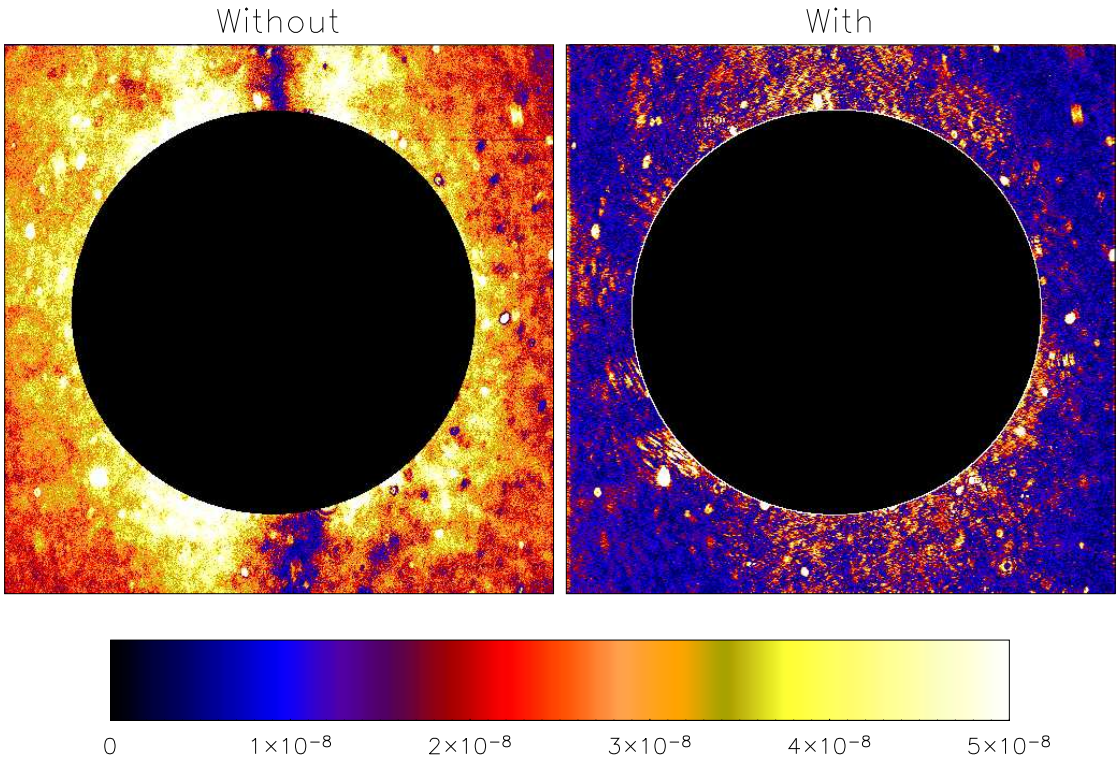

Figure 6: Effect of data analysis on the jitter correction. The left image is without jitter correction, and the right image is with the jitter removed.

is fitted to the matrix to determine the position x_0, y_0 of maximum correlation.

Another effect which can move the image on the detector is the polarizer. If the front and back of the polarizer are not perfectly co-planar, the image will move in a small circular motion on the detector as the polarizer is rotated. To isolate the effect of jitter from this "polarizer wedge" effect, only data with constant polarizer position was examined.

It was found that jitter could cause the image to shift by as much as 4 pixels peak-to-peak. The typical jitter was on the order of 1 pixel RMS in right ascension and about 0.5 pixels RMS in declination. It's critical for the polarization analysis to remove this jitter, as is demonstrated in Figure 6.

4.2 Polarizer wedge

A similar process can be used to explore the "polarizer wedge" effect. The mask is reversed to retain the bright rings around the edge of the occulter, while removing the scattered light pattern beyond the occulter. The result for the Polarcor polarizer is shown in Figure 7, where a clear circular pattern can be seen, with a radius of about 0.5 pixels. The other two polarizers showed similar behavior. Since the derived wedge effect is on the same order of magnitude as the random jitter component, it's most effective to treat both effects simultaneously with the jitter correction technique outlined in section 4.1. This procedure was followed in Figure 6.

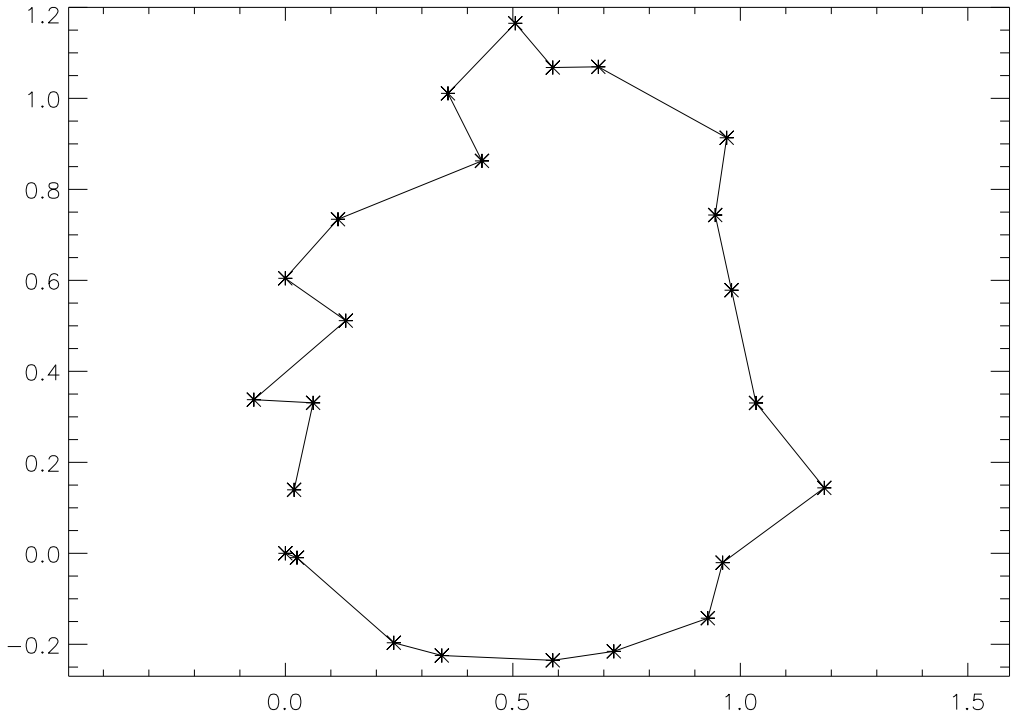

Figure 7: Relative occulter edge alignment in pixels between images taken with the polarizer rotated by 15° between exposures.

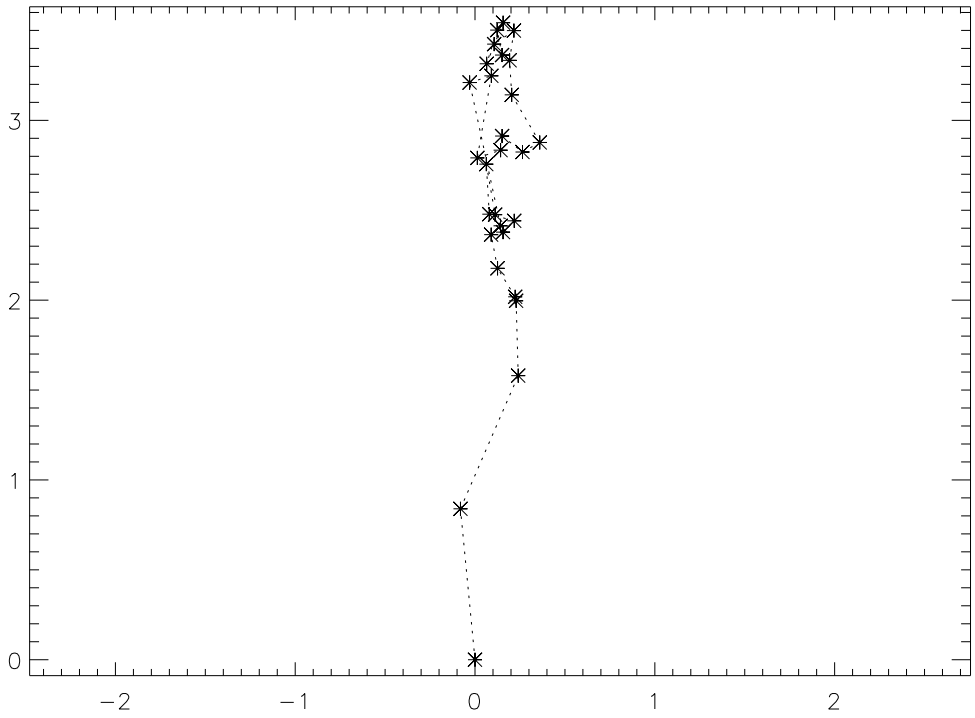

Figure 8: Drift of the bright rings on the detector with time. The axes are in pixels. The first observation is at the origin, and the subsequent observations drift upward.

4.3 Thermal motions

There also appear to be motions on the detector which cannot be explained as either jitter or polarizer wedge effects. This is demonstrated in Figure 8, where the rings around the edge of the occulter were tracked as a function of time. The polarizer was removed during these observations, so there is no effect from the polarizer wedge. Also, as explained earlier, instrument jitter does not affect the position of the rings on the detector. Therefore, this must be a completely separate motion, possibly due to a thermal effect. What is not known is whether this represents a motion of the occulter itself, or a flexing of the optical rail. The largest offset seen during the observing run was $\sim$4 pixels ($\sim 100\mu$m).

5 Comparing polarizers

As stated before, three different polarizers were tested. The results from each are demonstrated in Figure 9. The Polarcor polarizer showed linear striations in the polarized brightness images. These features showed wave-like motions when the polarizer was rotated, but did not themselves rotate. It's not clear what caused these features, but one possibility is reflections off of the polarizer housing. Because of cost requirements, the Polarcor polarizer was significantly smaller than what the flight design calls for. The other two polarizers were larger than the flight design.

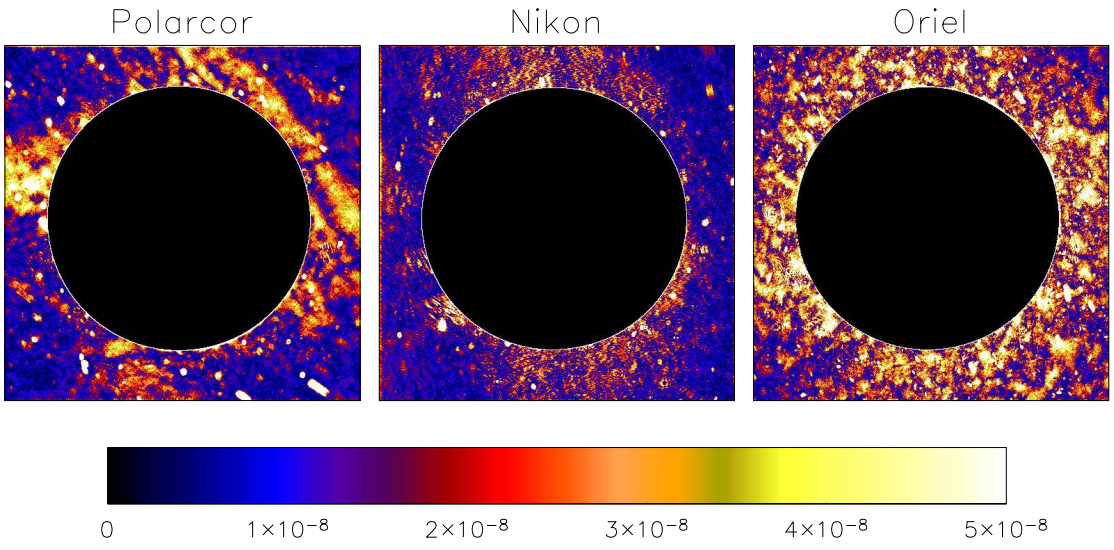

Figure 9: Polarized brightness derived from each of the three polarizers.

The Oriel polarizer, which was used in previous ETU tests, did not show the kind of organized features seen with the undersized Polarcor polarizer. Instead, there is an irregular background ranging from 1 to $4 \times 10^{-8} B/B_{\odot}$.

The most successful results were with a Nikon polarizer borrowed off of one of the Mauna Loa observer's cameras. This was a circular polarizer, consisting of a linear polarizer on one side, and a quarter-wave plate on the other. The linear polarizer side was placed facing the Sun. The average background outside apparent features was $\sim 10^{-8} B/B_{\odot}$ (Figure 10), or about 0.5% of the overall light level. These numbers are about a factor of two higher than the expected Poisson noise levels. (The Poisson noise during flight will be much lower, because the overall scattered light level will be lower, and the exposure time higher.)

In order to extract the polarized brightness, three images are needed at polarization angles spaced either 60° or 120° apart. The polarized brightness can then be derived as

$$pB = \frac{4}{3}\sqrt{(I_a + I_b + I_c)^2 - 3(I_a I_b + I_a I_c + I_b I_c)} \tag{2}$$

All possible image trios with the Nikon polarizer were examined to see which sets had sufficiently stable scattered light patterns to extract polarized brightness. A total of 32 sets was found. All but one of these sets were from a single 40 minute period, when the scattered light pattern remained constant. Most of these sets were taken at polarizer angles of 0°, 120°, and 240°. One way to beat down the noise in the data is to average together the data at each polarizer angle before applying Eq. 2. An alternative, but less successful, approach is to analyze each image trio separately, and then average the results together. The results from both methods are shown in Figure 11.

There is a circular "bull's eye" artifact visible at the top of Figure 11a (and to a lesser extent in Figure 11b) which is not seen in Figure 9. This feature shows up at a polarizer positions near 240°, and is believed to be a reflection off of the polarizer, possibly of doublet 1 with its attached Lyot spot. A similar artifact shows up in the data taken with the Polarcor polarizer, at a different position. Figure 11c shows the average of all image trios that don't include 240°.

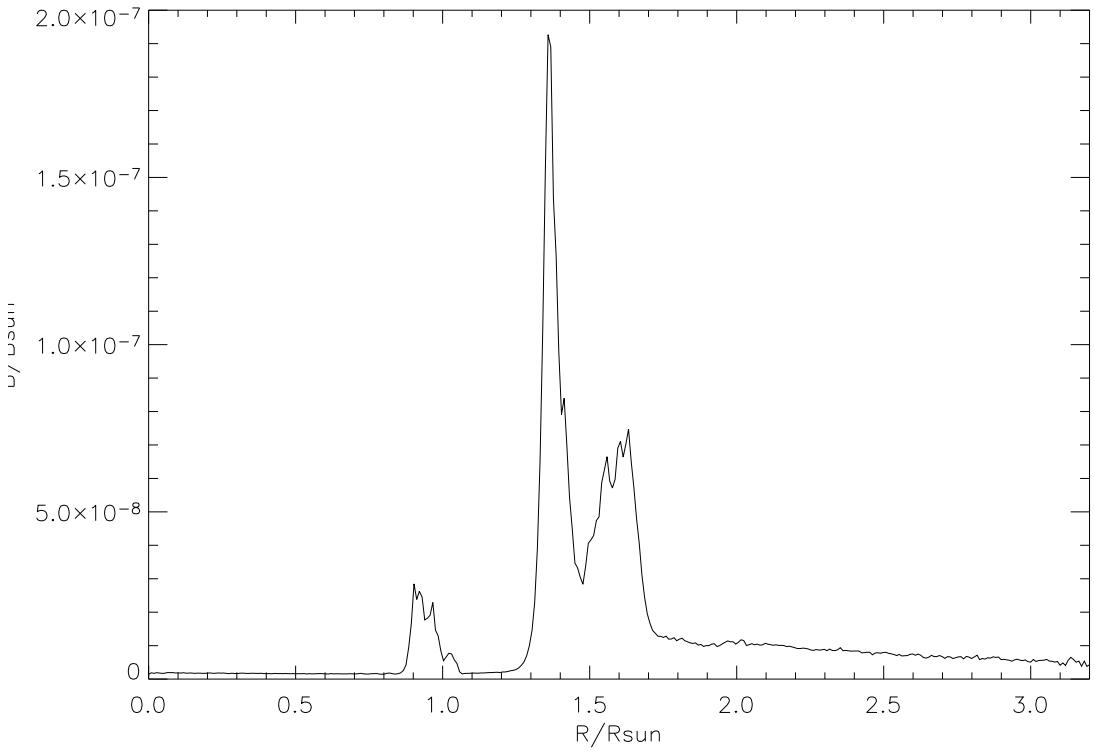

Figure 10: Estimated background level with the Nikon polarizer, as a function of radial distance.

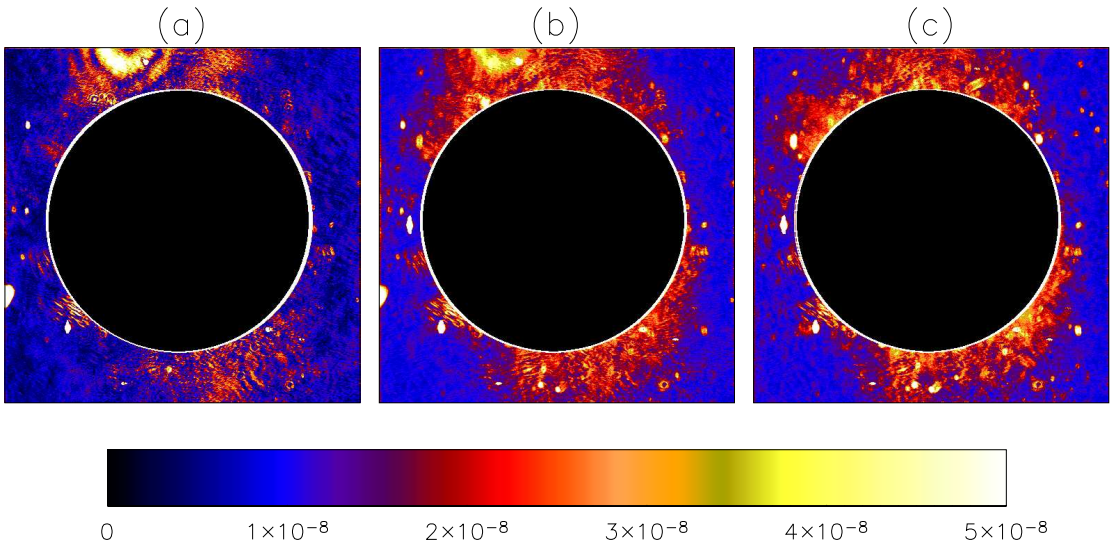

Figure 11: a) Polarized brightness derived by averaging together images at polarizer positions 0°, 120°, and 240° before applying the analysis. b) Polarized brightness derived by averaging together all possible image trios. c) Polarized brightness derived from averaging together all possible trios not including 240°.

6 Jitter correction sensitivity

Of the 32 image sets that were identified as yielding suitable measurements of polarized brightness, only two appear clean without applying a jitter correction. A critical question then is whether the results are highly sensitive to the parameters of the jitter correction.

When Eq. 1 is fitted to the cross-correlation matrix between images, one of the outputs is the formal uncertainty. Typically, this is on the order of 0.01 pixels. When three images are intercompared, each can serve as the master to be compared to the other two, giving three different results for the relative alignment. The difference between these results is much smaller than the formal error, at about 0.002 pixels.

To explore how the accuracy of the jitter correction affects the results, we applied the polarization analysis with images offset from their nominal positions by amounts ranging from 0.002 to 2 pixels. We found that the results are relatively insensitive to errors in the jitter analysis. Only when the jitter error is a significant fraction of a pixel does it start to meaningly affect the result. For small jitter errors, we found that the induced level of polarized brightness varied linearly with the error in the jitter correction. For example, an error of 0.002 pixels induced a polarized brightness error of $\sim 3 \times 10^{-11} B/B_{\odot}$. At 0.02 pixels, this grew linearly to $\sim 3 \times 10^{-10} B/B_{\odot}$.

These numbers are not directly applicable to what can be expected during flight, as it depends upon the gradient in the image, and the overall brightness level. However, the basic behavior is expected to be about the same. Thus, it's necessary to remove the jitter to the sub-pixel level—both to retain the instrument resolution, and to not introduce spurious signal in the pB analysis—but extreme accuracy is not required.

7 Intrinsic noise

One way to estimate the intrinsic noise in the results is to apply the polarization analysis of Eq. 2 to image trios where the polarizer angle was held constant. With perfect data, this technique would return zero polarization. With noisy data, the apparant polarized brightness images represent the noise inherent in the data. When this technique is applied to the data used to generate Figure 11a, a very similar image is produced, as shown in Figure 12. This suggests that the signal-to-noise ratio is not sufficient to distinguish the coronal signal. The values in Figure 12 are consistent with those plotted in Figure 10.

Except for the "bull's eye" artifact discussed earlier, there's a strong correlation between the false polarized brightness image shown in Figure 12 (or the images in Figure 11) and the instrument scattering profile in Figure 3, which is taken from the same data. There are several possible reasons why this would be. For example, if the detector response varied between images, then the residuals would be higher where the scattered light was higher. One way this could come about if the shutter performance varied slightly between exposures. If the shutter was only accurate to ∼0.5% RMS, then that would be sufficient to explain the residuals in the data. In fact, the exposure time used (0.02 s) was just above the smallest exposure time that the non-flight Apogee camera is capable of.

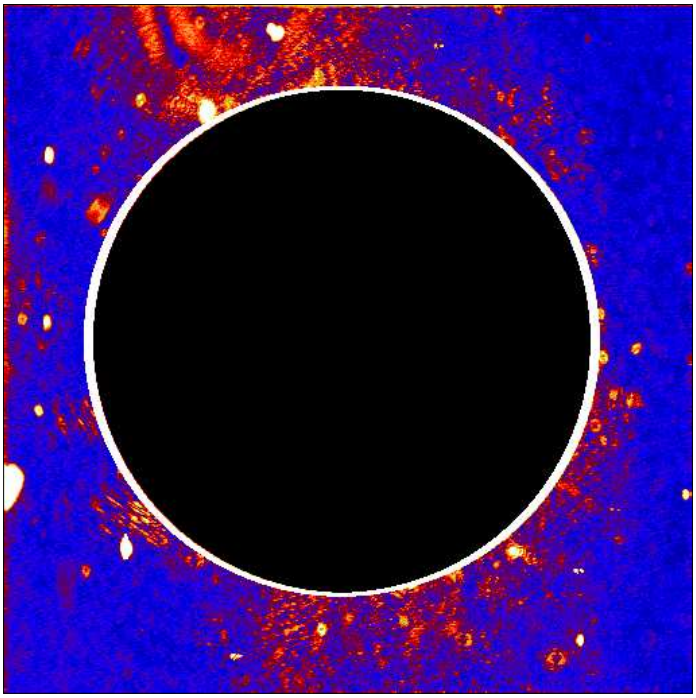

Figure 12: Average scattered light pattern produced by analyzing trios of images taken at a constant polarization angle. The color scale is the same as in Figure 11.

8 Comparison with MLSO Mark IV data

Figure 13 shows the comparison of the data from Figure 11a to simultaneous data taken with the MLSO Mark IV. It's evident that there's no obvious correlation between features.

It should be noted that the relative calibration between the Mark IV and the ETU is not exact. Conservatively, the calibration procedure discussed in Section 2 can only be considered to be good to $\sim$30%, given that the transmission of the neutral density filter is only theoretical, and that the filter and diffuser were never measured as a unit. The color table in Figure 13 and other figures was chosen to emphasize the most evident features, and is sensitive to the calibration. Thus, it may appear in Figure 13 that there are features in the Mark IV data which are brighter than their corresponding locations in the ETU data, but this could simply be an artifact of the relative calibration.

In Section 7, it was suggested that the exposure time might not be entirely consistent between exposures. To test this, we tried renormalizing the three images before applying Eq. 2. The Mark IV data shows almost no coronal emission in the lower-right corner of the ETU image, so the average in a box 150×100 pixels wide was used to renormalize the data. The results are shown in Figure 14. (Note that the color table is different from previous figures, to bring out the fainter features.) These data are quieter than previous data, with fewer evident features. Also, one can start to see areas of emission which may match coronal features in the Mark IV data. These possible coronal features are marked by arrows. However, there are still other features in the data which are clearly not coronal, and which are brighter than the coronal features. Also, the noise baseline is still consistent with that shown in Figure 10.

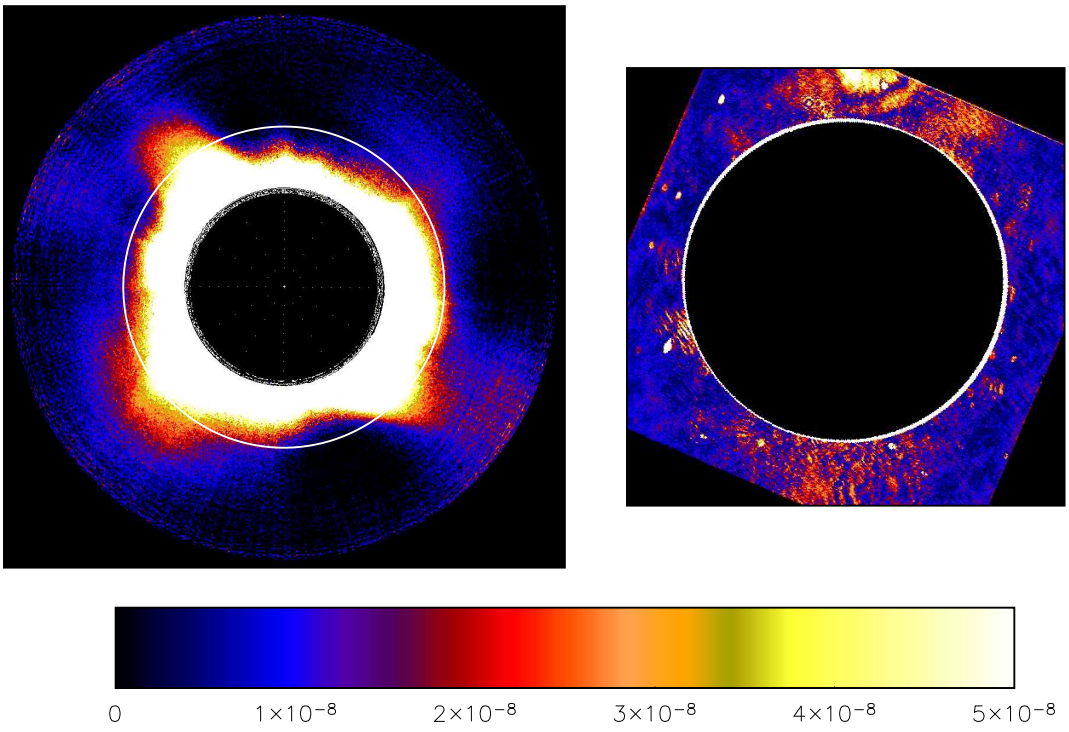

Figure 13: Comparison of data taken with the MLSO Mark IV coronagraph with the data from Figure 11a, which has been rotated by the solar P_0 angle of 23.4°.

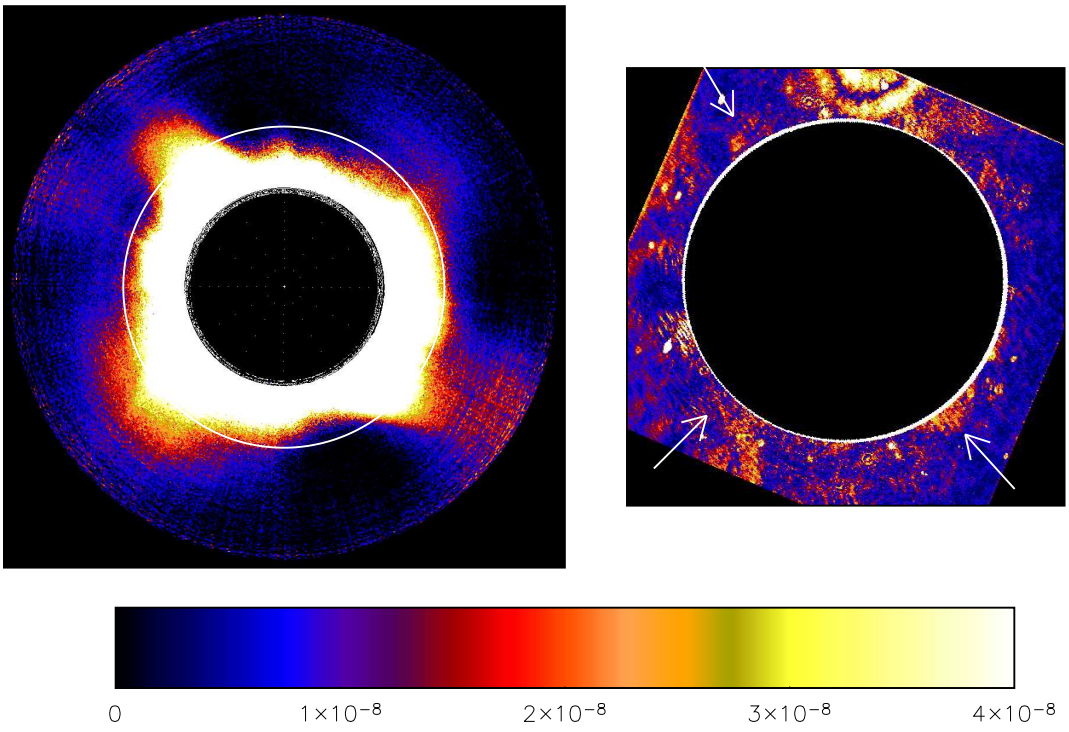

Figure 14: Same as Figure 13, but with the data renormalized before applying Eq. 2. Arrows point to possible coronal emission. The color table has been enhanced to bring out the fainter features.

9 Conclusions

In many ways, using the instrument at Mauna Loa proved to be much more difficult than is expected for the flight instruments. The non-flight issues that we ran into were as follows:

- The atmospheric scattering was significantly higher than the intrinsic scattering of a clean objective lens, lowering the expected signal-to-noise ratio.
- Because of technical difficulties and schedule considerations, the instrument did not have a focal plane mask. Because of the additional atmospheric scattering, this did not drive the signal-to-noise, but it did limit the depth to which the solar atmosphere could be probed.
- The instrument scattering profile was varying with time, as dust fell onto the objective lens. This limited the number of observations to those periods where no extra dust fell on the objective.
- The pointing spar showed considerable jitter, which needed to be removed before the data could be used. It's possible that we did not have the sun sensor on the spar tuned to its optimal capabilities.
- The shutter stability on the Apogee cameras may not have been sufficient to probe all the way down to the Poisson noise of the cooled CCD. The flight specification calls for a stability of 10^-3.

Also, without the long baseline of observations possible in flight, one cannot build up a knowledge of the instrumental profile independent of the coronal features. In particular, one cannot roll the instrument to separate the instrumental features from the corona.

Of the three polarizers tested, the only one that produced good data was the borrowed Nikon polarizer. An important question is whether the problems seen with the Polarcor polarizer are a flight issue, or were due to the polarizer being too small. This is currently under investigation.

We established that the instrument is sensitive to jitter between exposures. However, the alignment requirements are not so tight that the jitter cannot be removed.

The alignment of the image on the detector showed drifts of as much as 4 pixels (100 μm), which could not be attributed either to jitter or polarizer rotation. It's theorized that these motions were thermally generated. What's not known is whether these motions were due to changes in the occulter stem, or in the Newport rail that the instrument was attached to.

When all known corrections are applied to the data, the noise level is close to $1.2 \times 10^{-8} B/B_\odot$ near the edge of the occulter, decreasing to about $5 \times 10^{-9} B/B_\odot$ at three solar radii. This represents about 0.5% of the scattered light level, and can be as much as twice that due to Poisson statistics alone. Some features were seen which may be coronal in origin, but are combined with other features which are clearly instrumental.

The use of the calibration window in the COR1 door was demonstrated.

Acknowledgments

The authors wish to thank the MLSO observers, Darryl Koon, Allen Stueben, and Eric Yasukawa, without whom we could never have done this. We also wish to thank Darryl for the use of his Nikon polarizer. Particular thanks go to Greg Card, who came out to Goddard before the instrument was shipped to test the interface with the HAO pointing spar.